Radio Channel Models for Search-and-Rescue Missions into Collapsed Structures

Claude Oestges

ICTEAM Electrical Engineering, Université catholique de Louvain
3 place du Levant, 1348 Louvain-la-Neuve, BELGIUM
claude.oestges@uclouvain.be

***Abstract*— Propagation models in the TETRA/GSM/UMTS bands (from 433 MHz to 1.9 GHz) in partially destroyed buildings are derived, using a number of methods with respect to various collapsed structures. These models are useful in the context of pedestrian radio-localization systems relying on cell phone signals. In addition, the electromagnetic properties of concrete and ferro-concrete materials are experimentally characterized and used in the various models. Simulations show that specific attenuation levels can be very severe, from 10 to 100 dB/m, and increase with frequency. This might seriously limit the detection of victims under more than one meter of ferro-concrete rubbles in the UMTS band. However, localization algorithms based on direction-of-arrival estimation are unlikely to be degraded by multipath spreading.**

I. INTRODUCTION

The retrieval of people trapped in buildings in fire or partially destroyed is a priority for rescue teams. A first microwave life-detection system was proposed by [1]. The goal was to remotely observe the physiological status of a wounded subject lying on the ground, at a maximum distance of 30 m or behind barriers. Continuous wave (CW) radar at 10 GHz was used to illuminate the patient and the presence of breathing and heart beating modulates the signal. This modulation is then extracted from the received signal. The localization of human beings behind rubbles using the X band was also investigated in [2]. Body movements were detected at distances of 3 to 5 m without any obstacle and of 2 m behind a concrete wall. The system was improved in [3] by using a triple frequency radar, at 10 GHz, 2.45 GHz and 433 MHz, as to overcome the high attenuation in the X band. Attenuations of 60 to 100 dB were measured at 2.45 GHz (compared to more than 250 dB at 10 GHz).

Given the widespread use of mobile phones by the general public, an innovative idea to retrieve victims or to track rescue teams [4] consists in capturing, via an antenna array acting as subrogated base station, the signals transmitted by cell phones (even if these are in idle mode). Real-time post-processing then allows localizing the victim using a robust localization algorithm. The receive antenna array may be mounted under a helicopter for a first rough localization, while a second step involves a pedestrian rescue team equipped with portable versions of the same antenna array, providing in real-time localization data of the victim. In order to evaluate the performance of localization algorithms, a precise channel characterization is however required.

Collapsed building structures constitute a very complex environment, for which existing models are scarce. Also, there is a huge variety of possible scenarios because

- many different materials can be involved,
- the electromagnetic properties of any given material strongly depends on the structure, humidity, compression, etc., so that the values of permittivity and conductivity are hardly known with precision,
- the shape and dimensions of each rubble is highly variable.

In this paper, we propose modelling approaches for three types of collapsed structures, namely layered, spherical- and non-parallel slab-based.

II. MATERIAL CHARACTERIZATION

A. Literature Overview

Each material is characterized by its permittivity and conductivity, as given by Table I [5]–[9]. Regarding concrete, there is a large spread of values, as indicated by the range of values. For ferro-concrete, there is little information available in terms of complex permittivity. Hence, it is further addressed in the next section.

TABLE I
COMPLEX PERMITTIVITY OF VARIOUS MATERIALS

Material	1 GHz	2 GHz
Brick	$3.8 - 0.14j$	$3.8 - 0.27j$
Concrete	$[5...9] - [0.4 ... 0.7]\,j$	$[5...9] - [0.4 ... 0.7]\,j$
Stone	$6.5 - 0.54j$	$6.5 - 0.3j$
Glass	5.5	5.5
Wood	$2.5 - 0.40j$	$2.5 - 0.50j$

B. Experimental Characterization

1) Measurement Set-Up: To verify the above values or to fill gaps in the list of materials/frequencies, an experimental set-up has been developed at UCL. It consists in measuring the transfer function over a large frequency bandwidth of a material slab. The measurement is performed by means of an vector network analyzer, whose input and output are linked to identical transmit and receive horn antennas. The determination of the permittivity and conductivity based on the complex transfer function (S_{21} parameter) nevertheless requires an additional calibration to

- de-embed the effects of antenna and mounting structure effects [10],

- remove internal multipaths.

This calibration implies namely to estimate the coordinates of the antenna reference planes, the size of the Fresnel zones, etc.

2) Results for Concrete and Ferro-Concrete: The experimental slabs are circular disks, of a few cm thickness. The ferro-concrete slab contains radial horizontal metallic rods (i.e. the rods are perpendicular to the transmission axis).

Figure 1 illustrates that the ferro-concrete slabs attenuate from 8 to 10 dB more on the 2-6 GHz, and we may safely interpolate that the same difference will be observed at 1 GHz. From the above graph, we may extract the complex permittivity of both materials. The results are illustrated in Figure 2. We notice that the real part of the permittivity is rather insensitive to the presence of the metallic rods. It is equal on the average to 9 over the whole frequency range. This is relatively smaller then the values measured by [5] and [9], but in good agreement with the values measured by [11]. By contrast, the loss tangent is much larger for the ferro-concrete slab, especially below 3 GHz, where it can reach 0.4.

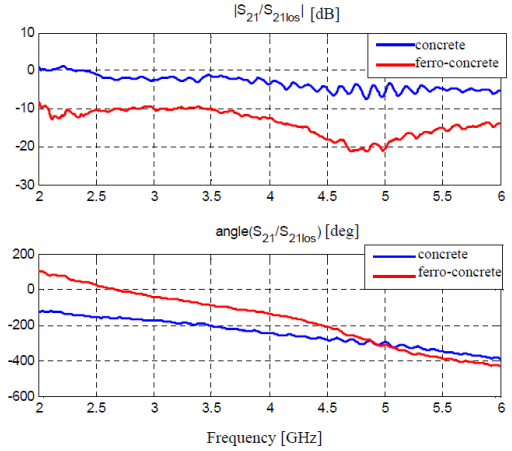

Fig. 1. Measured transmission in concrete and ferro-concrete slabs, relative to line-of-sight (LOS): amplitude (top) and phase (bottom).

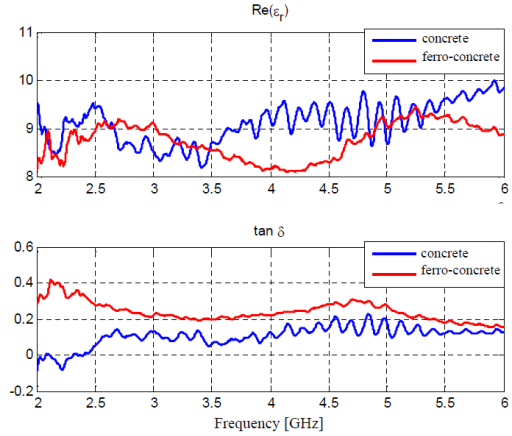

Fig. 2. Estimated complex relative permittivity of concrete and ferro-concrete: real part (top) and loss tangent (bottom).

Hence, we consider a complex permittivity for concrete to of $9 - 0.4j$ and $9 - 0.5j$ at 1 and 2 GHz respectively, and for ferro-concrete, of $8.5 - 1.8j$ and $8.5 - 2.55j$ at 1 and 2 GHz respectively.

III. Layered Structures

A. Modeling Assumptions

The model relies on the hypothesis of stratified rubbles. In the model, the collapsed structure is thus made of several layers, each layer being characterized by the electromagnetic properties of its constituent and by its thickness. The geometry of the medium is represented in Figure 4. The medium is made of $N+1$ layers, indexed by $k = 0, \ldots, N$, of respective thickness h_k. Considering that the rescuer's antenna is represented by a punctual receiver, it is naturally possible to calculate the electromagnetic fields **E** and **H** impinging on the base station for any position of the terminal in the multi-layered medium [12]. However, because the terminal is buried in the medium, it is not rigorous to consider plane waves. Hence, Maxwell's equations must be solved in spherical coordinates. The numerical solution to the above problem is calculated by means of the tool developed in [12] which was adapted to fit the specific configuration.

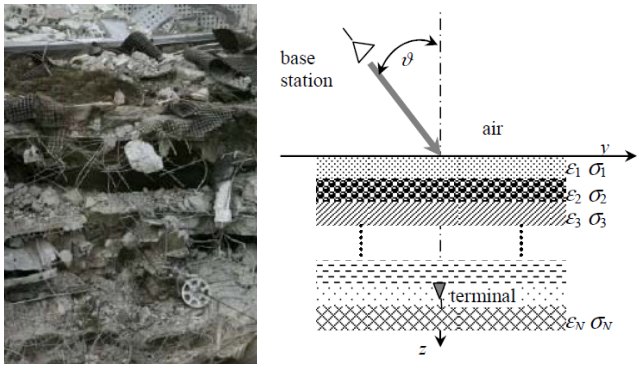

Fig. 3. A collapsed structure (left) and its representation as a multi-layer medium (right).

B. Simulation Results

In simulations, the ordering of the layers, as well as their respective thickness, are taken as random variables to obtain meaningful statistical results. We consider operating frequencies of 1 and 2 GHz, as well as up to five materials, each time present in equal proportions: brick, stone, concrete, ferro-concrete and wood.

The thickness of the layers is considered as Gaussian distributed, with a mean of 50 cm and a standard deviation of 20 cm. A second set of results is obtained for layers of average thickness of 20 cm, with a standard deviation of 5 cm. Without ferro-concrete, the mean specific excess attenuations reach 8 and 20 dB/m at 1 and 2 GHz respectively, with standard deviations on the integrated excess attenuation from 2 to 10 dB depending on the mean thickness of the layers. When ferro-concrete layers are included (in the same proportion as other layers), specific attenuation reach respectively 14 and 31 dB/m, with standard deviations from 2 to 14 dB depending on the mean thickness of the layers.

The layered model validated by means of measurements on a 3-layer test-structure, made of two outer layers of ferro-concrete (6-cm wide) and one intermediate layer made of a

mix of air and ferro-concrete (12-cm wide). For this set-up, the simulated and measured attenuation at 2 GHz are 72 and 80 dB/m respectively. This is much higher than the simulations above, given the fairly high proportion of ferro-concrete (around 75 %).

IV. Spherical Scatterer-Based Structures

A. Modeling Assumptions

In this second scenario, we consider heavily destroyed structures, such that only rubbles subsist. An illustration of such scenario is depicted in Fig. 4. Obviously, it might not be straightforward to represent this scenario by means of a layered model. Therefore, rubbles are considered as spherical scatterers. For a population of inhomogeneous spheres, we consider a slab of thickness d containing a large number of spherical scatters of different material and different sizes (see Fig. 4). We further introduce a set of materials, indexed by m, as well as a probability of occurrence for each material:

$$p_m = \frac{\text{number of spheres of material } m}{\text{total number of spheres}} \quad , \quad \sum p_m = 1 \qquad (1)$$

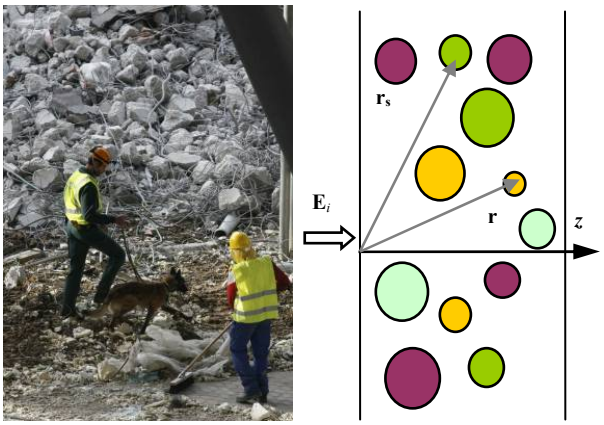

Fig. 4. A collapsed structure (left) and its representation as a population of spherical scatterers (right).

Let us define $n_m(a)$ as the size distribution, i.e. the probability (such that its integral is equal to 1) for a m-material sphere to have a radius equal to a. The number of spheres per unit volume of radius a and material m is given by $p_m N_m(a)\,da = p_m n_m(a) K\,da$, the constant K being determined by fixing a filling factor η,

$$\eta = \sum_m \int_0^\infty p_m N_m(a) \frac{4}{3}\pi a^3 da \,. \qquad (2)$$

The attenuation is obtained by integrating over all spheres, considering that scattering does not contribute to a loss (i.e. that the scattered power is strongly oriented in the forward direction, so that the loss results from absorption only):

$$A[\text{dB/ m}] = 20\log\left[\sum_m \int_0^\infty p_m N_m(a)\sigma_m(a)\,da\right], \qquad (3)$$

where $\sigma_m(a)$ is the absorption cross-section for a m-material sphere of radius a, which can be calculated as a function of the complex permittivity.

B. Simulation Results

Considering a mixed population of spheres with 70 % of concrete (the remaining 30 % consisting of glass, brick, wood and metal), the specific attenuation in [dB/m] can be fitted as $\alpha\eta$, with α depending on the size distributions. Typical values for α range from 35 to 45.

V. Non-Parallel Slab-Based Structures

In this last model, we want to estimate the attenuation in scenarios such those represented in Fig. 5. Given the large variety of structures, we investigate a so-called canonical scenario, described in Section V.A, and apply an asymptotic ray-tracing tool to predict the attenuation and the direction-of-arrival of the main contribution.

Fig. 5. Two typical non-parallel slab-based structures.

A. Canonical Scenario

The canonical scenario used in this study is represented in Fig. 6. Note that layers 2 and 4 are parallel, in order to account for guided propagation effects.

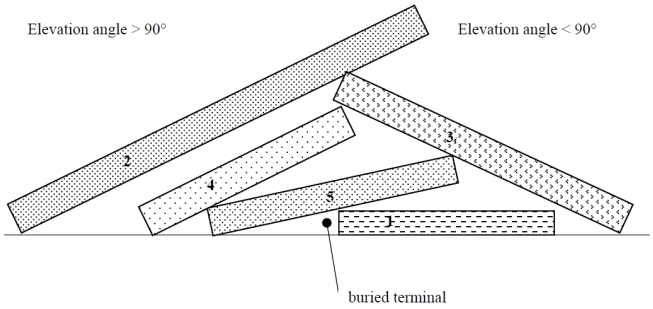

Fig. 6. Canonical representation of non-parallel slabs.

A thickness of 32 cm is considered for all layers, except for layer 4, whose thickness is 20 cm. This choice is made as to allow for the largest number of possible interactions in this canonical scenario.

B. Ray-Based Model

To estimate the global attenuation and the direction-of-arrival of the waves transmitted by the buried terminal, we assume that law of geometrical optics hold true and trace back all directly-transmitted, reflected and diffracted rays linking the buried terminal to the base station. The amplitude of any

ray is then expressed, for a single contribution *m* (i.e. with one reflection or one diffraction only), as [13]:

$$\mathbf{E}_m = \frac{K'_m(s,s')\ e^{-jks'} \cdot \mathbf{T}_m \cdot K_m(s,s')\ e^{-jks}}{\prod_n L_n}\mathbf{E}_0 \qquad (4)$$

where

- $\mathbf{E}_0$ is the emitted vector field (k being the wave number),
- s and s' are the path lengths from the transmitter to the reflecting surface or the diffracting wedge, and from the surface/wedge to the receiver,
- K_m and K'_m are respectively the free-space transmitter-obstacle and obstacle-receiver spreading factors,
- $\mathbf{T}_m$ is the dyadic complex coefficient modeling the interaction mechanism responsible for the considered contribution,
- $\prod_n L_n$ is the penetration loss of each crossed slab.

C. Simulation Results

The following table illustrates the path attenuation (relative to line-of-sight) for different rays (T: transmission through slabs, R: reflected: D: diffracted), considering concrete or ferro-concrete slabs and different base station locations (angles are chosen to maximize the number of possible interactions). It can be seen that the obstructed line-of-sight is always the lower attenuated path. However, for ferro-concrete slabs, this attenuation is again extremely large.

TABLE II
RAY ATTENUATION [DB] FOR CONCRETE/FERRO-CONCRETE SLABS

	Path description	1 GHz	2 GHz
Elevation angle of 146° (left side)	T2 T4 T5	6.3/28.3	12.4/79.7
	T2 R4 R2 T4 T5	11.6/33.7	17.7/85.0
	T2 R4 R2 R4 R2 T4 T5	16.8/39.0	22.9/90.2
	T2 D3 T4 T5	26.9/49.0	34.5/102.1
Elevation angle of 90°	D2 T3 T4 T5	21.8/41.5	28.2/88.3
	T2 T3 T4 T5	7.7/35.1	15.3/99.0
	T2 D3 T4 T5	23.1/42.7	29.7/89.4
Elevation angle of 56° (right side)	T3 T5	4.9/22.0	9.6/61.8
	T3 D4 T5	21.3/38.6	27.0/79.6
	D2 D2 T3 T4 T5	25.2/51.2	33.8/112.9

VI. PERSPECTIVES AND CONCLUSIONS

In this paper, we have investigated three propagation scenarios corresponding to different collapsed structures, and proposed adequate models to predict the attenuation and the angular spreading of waves transmitted by a buried terminal. In all cases, the obstructed line-of-sight is the dominant contribution, which guarantees that a direction finding algorithm would perform satisfactorily. In terms of attenuation and detection range, let us consider that the dynamic range of 2G+ and 3G handsets is limited by a maximum transmit power of 1 W (30 dBm) and a receive sensitivity of 102 dBm, which yields a dynamic range of approximately 130 dB. According to structure material, the detection range is limited as illustrated in Table III.

TABLE III
DETECTION RANGE IN TYPICAL SCENARIOS

Material	TETRA	GSM-900	UMTS
Free-space	> 5 km	> 5 km	> 5 km
Concrete + mixed	~ 15 m	~ 10 m	~ 4 m
Ferro-concrete	< 3 m	< 2 m	< 1 m

Field-trials [4] show that the detection and location of GSM handsets (at 900 MHz) could be performed through three ferro-concrete walls of 25 cm thickness each (0.75 m in total). Regarding ferro-concrete blocks, the attenuation can become very high (60 to 80 dB) and drastically limits the use of localization system, at least for GSM-1800 and UMTS frequencies.

ACKNOWLEDGMENT

Claude Oestges is pleased to acknowledge the financial support of the Belgian Fonds de la Recherche Scientifique. Part of this work was also carried out within FP6 research contract STARRS (IST-2005-33742).

REFERENCES

[1] K-M Chen, et al., "An X-band microwave life-detection system," *IEEE Trans. Biomedical Eng*., vol. 33, no. 7, pp. 697-701, July1986.

[2] E.G. Aggelopoulos, *et al.*, "Mobile microwave sensor for detection of trapped human beings," *Measurement*, vol. 18-3, pp. 177-183, 1996.

[3] M. Bimpas, *et al.*, "Development and testing of a detector system for trapped humans in building ruins," in *Proc. EuMC 2003*, pp. 999-1002, 2003.

[4] P. Morgand *et al*., "Detection and location of people in emergency situations through their PMR or GSM/UMTS phones," in *Proc. EuWIT 2010*, pp. 185-188, September 2010.

[5] I. Cuinas, M.G. Sanchez, "Measuring, modelling and characterization of indoor radio channel at 5.8 GHz," *IEEE Trans. Veh. Technol.*, vol. 50, no. 2, pp. 526-535, March 2001.

[6] D. Pena, *et al*., "Measurement and modelling of propagation losses in brick and concrete walls for the 900 MHz band", *IEEE Trans. Antennas and Prop*., vol. 51, no. 1, pp. 31-39, Jan. 2003.

[7] R. A. Dalke, *et al*., "Effects of reinforced concrete structures on RF communications", *IEEE Trans. on Electromagnetic Compatibility*, vol. 42, no. 4, pp. 486-496, 2000.

[8] E. Richalot, *et al*., "Electromagnetic propagation into reinforced-concrete walls," *IEEE Trans. Microwave Theory Tech.*, vol. 48, pp. 357-366, Mar. 2000.

[9] B. De Backer, *et al*, "Propagation mechanisms for UHF wave transmission through walls and windows," *IEEE Trans. Veh. Techn.*, vol. 52, no.5, pp. 1297-1307, Sep. 2003.

[10] S. Lambot *et al*., Estimating soil electric properties from monostatic ground-penetrating radar signal inversion in the frequency domain, *Water Resources Research*, n° 40, 2004.

[11] H. Suzuki and A.S. Mohan, "Measurement and prediction of high spatial resolution indoor channel characteristic map," *IEEE Trans. Veh. Technol.*, vol. 49, no.4, pp. 1321-1333, July 2000.

[12] I. van den Bosch, "Accurate modeling of GPR for detection and signature extraction of mine-like targets buried in stratified media," Ph.D. thesis, Université catholique de Louvain, 2006.

[13] F. Mani, *et al.*, "Accuracy of depolarization and delay spread predictions using advanced ray-based modeling in indoor scenarios," *EURASIP Journal on Wireless Comm. and Networking*, 2011.